

communications

earth & environment

ARTICLE



<https://doi.org/10.1038/s43247-021-00242-3>

OPEN

High geothermal heat flow beneath Thwaites Glacier in West Antarctica inferred from aeromagnetic data

Ricarda Dziadek^{1,2}, Fausto Ferraccioli^{3,4} & Karsten Gohl¹

Geothermal heat flow in the polar regions plays a crucial role in understanding ice-sheet dynamics and predictions of sea level rise. Continental-scale indirect estimates often have a low spatial resolution and yield largest discrepancies in West Antarctica. Here we analyse geophysical data to estimate geothermal heat flow in the Amundsen Sea Sector of West Antarctica. With Curie depth analysis based on a new magnetic anomaly grid compilation, we reveal variations in lithospheric thermal gradients. We show that the rapidly retreating Thwaites and Pope glaciers in particular are underlain by areas of largely elevated geothermal heat flow, which relates to the tectonic and magmatic history of the West Antarctic Rift System in this region. Our results imply that the behavior of this vulnerable sector of the West Antarctic Ice Sheet is strongly coupled to the dynamics of the underlying lithosphere.

¹ Alfred Wegener Institute Helmholtz-Centre for Polar and Marine Research, Bremerhaven, Germany. ² Department of Geosciences, University of Bremen, Bremen, Germany. ³ Istituto Nazionale di Oceanografia e di Geofisica Sperimentale, Sgonico TS, Italy. ⁴ British Antarctic Survey, Cambridge, UK.
✉ email: karsten.gohl@awi.de

The Amundsen Sea sector of West Antarctica (Fig. 1a, b) is the Earth's prime region to test hypotheses on the interacting relationship and coupling between the solid earth and the cryosphere. In this study, we examine the distribution of geothermal heat flow (GHF) as a key factor to reveal past and present geodynamic, tectonic, and lithospheric processes and their correlation to the presently observed enormous ice mass loss in this region.

Geothermal heat flow of the Antarctic continent is one of the essential geophysical parameters for both delineating and identifying tectonic and geodynamic features and processes, and improving the parameterization of basal conditions in ice-flow dynamic models. Apart from a few locations¹, thick ice cover and logistical challenges have largely prevented the installation of a dense network of direct temperature gradient measurement sites in drill holes, and will likely do so in the future. Indirect determination of heat flow from other geophysical parameters such as magnetic anomalies^{2,3}, seismological models^{4–6}, and interpretation of ice-penetrating radar images⁷ as well as the estimation of crustal heat production from exposed geological provinces⁸ have improved with greater coverage of data and accuracy of the models, and increasingly help relate tectonic and magmatic features to ice sheet dynamics.

The Amundsen Sea Embayment is underlain by the eastern branches of the West Antarctic Rift System, which extends from the Ross Sea to the Amundsen Sea and Bellingshausen Sea sectors of West Antarctica^{9–11}. Lithospheric and crustal properties, such as thin crust, thin elastic lithospheric thickness, and high uplift rates, as well as interpreted tectonic and magmatic features, such as individual rift basins, fault systems, and young volcanic activity, coincide with the presently observed largest ice mass loss in Antarctica (outside the northern Antarctic Peninsula) by rapid thinning and retreat of the Pine Island, Thwaites, Pope, and other glaciers in the embayment^{12–14}. This tectonic setting of the ASE is

likely to favor relative high geothermal heat flow. Continent-wide studies of geothermal heat flow derived from magnetic and seismological data consistently indicate a substantially higher geothermal heat flow of West Antarctica compared to that of East Antarctica^{2–5}. However, these continent-scales models still suffer from large uncertainties and lack the regional detail for the Amundsen Sea and other sectors.

Results and discussion

Curie depth distribution. The Curie depth is considered as a proxy for geothermal heat flow, because it represents the depth-to-bottom of a magnetic source in a first approximation of the temperature dependence of magnetization in crustal rocks (details are in Supplementary Method 1.1 to 1.3). We find that Curie depths (Fig. 2b) range between 10 and 18 km with the 580 °C isotherm dipping down towards Thurston Island. In the central part of the Thwaites and Pope glacier catchment systems, the Curie isotherm exhibits shallow depths of 12–16 km, propagating onto the Amundsen Sea Embayment shelf. Shallower 580 °C isotherms are located in the Byrd Subglacial Basin region and the southwestern part of the Bentley Subglacial Trench. The Pine Island Rift structure does not show prominent Curie depth anomalies, but indicates shallow thermal anomalies in the eastern part. Our estimates for the standard deviation of the Curie depth (Supplementary Fig. 3) is ±1 km for most of the study area and peaks with ±2.7 km in the magnetic basin between Thurston Island and Ellsworth–Whitmore Mountains, and towards Marie Byrd Land, where magnetic data coverage is poor. Further considerations are reported in Supplementary Method 1.3 and Supplementary Discussion 2.1. We note, that the shallow Curie depth distribution correlates well with volcanic centers (e.g., Mount Takahe), which are further indicative for presumed elevated crustal heat flow.

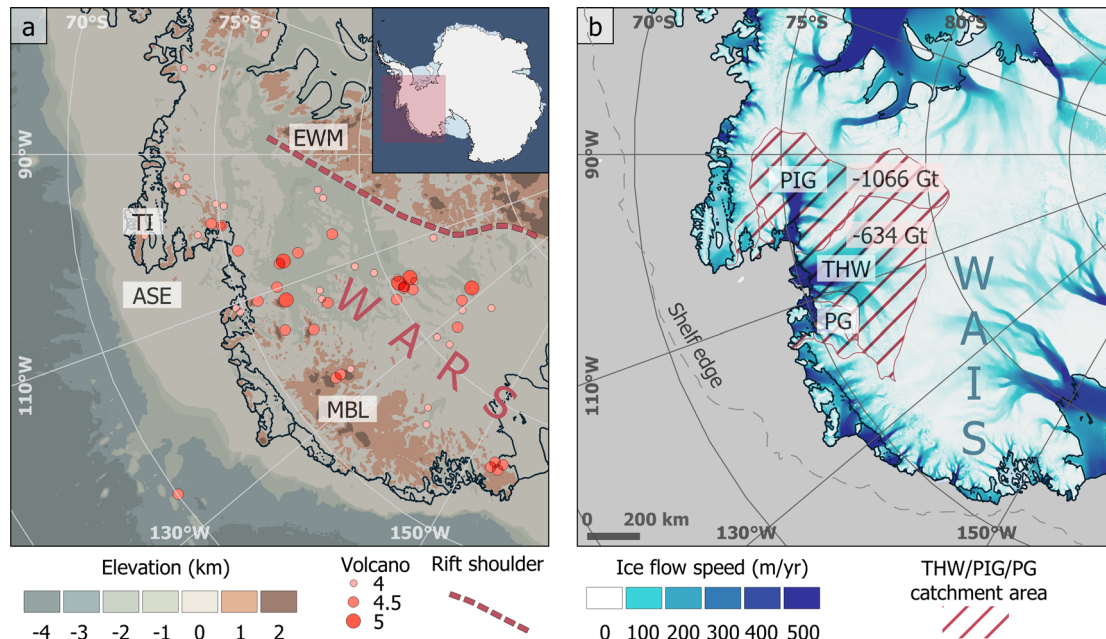


Fig. 1 Overview of the study region. a Map shows bed elevation⁵¹, rift shoulder of the West Antarctic Rift System (WARS), and locations of volcanoes²² with a confidence factor of 4 or higher. Highlighted area indicates study region. EWM Ellsworth-Whitmore Mountains, ASE Amundsen Sea Embayment, MBL Marie Byrd Land. **b** Catchment areas of Pine Island (PIG), Thwaites (THW), and Pope (PG) glaciers which drain the West Antarctic Ice Sheet (WAIS) into the Amundsen Sea Embayment. Present day ice flow velocities are amongst the highest in Antarctica^{52,53}. The cumulated ice mass loss of 4760 Gt for the Thwaites (THW) and Pine Island (PIG) catchment region over the last four decades (1979–2017) accounts for 36% of the total Antarctic ice mass loss¹⁴.

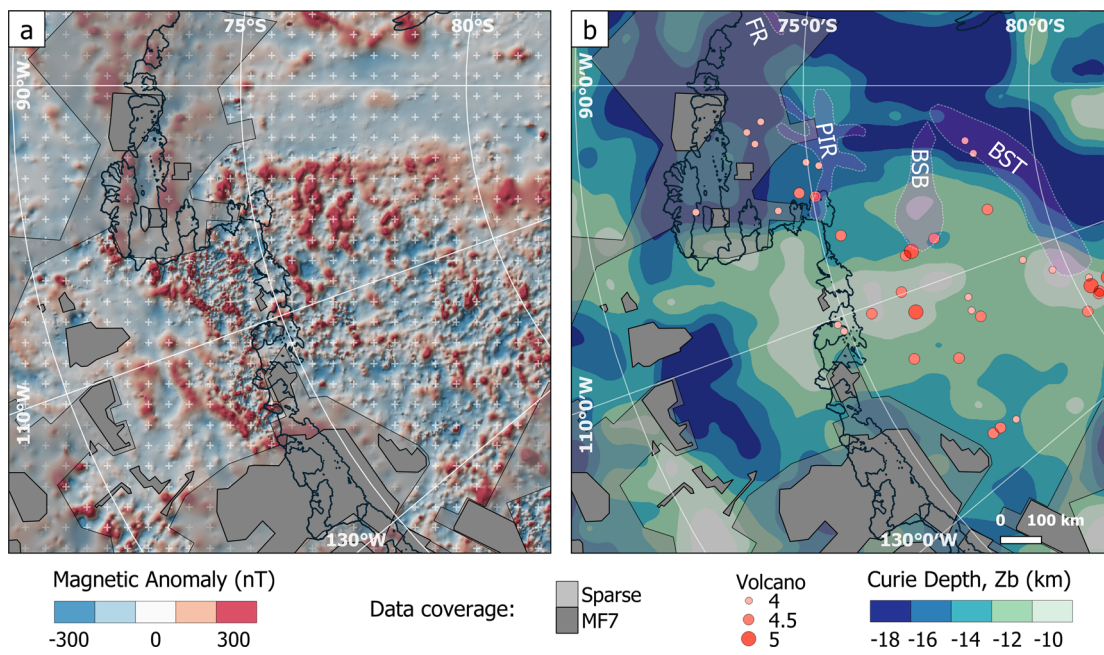


Fig. 2 New magnetic anomaly grid and Curie-depth estimates in the Amundsen Sea sector of West Antarctica. **a** Magnetic anomaly grid with areas with low magnetic data coverage indicated in light gray and areas, where data gaps have been substituted with MF7 satellite magnetic data (<https://www.geomag.us/models/MF7.html>) shown in dark gray. Small white crosses show locations of the 200×200 km window centers for the spectral analysis. **b** Curie-depth distribution and volcanic centers with a confidence factor of 4 or higher²². BSB Byrd subglacial basin, BST Bentley subglacial trench, FR Ferrigno rift, PIR Pine Island rift.

Geothermal heat flow. Our geothermal heat flow estimates (Fig. 3a), that assume a thermal conductivity of 2.2 W/mK , resemble the Curie depth distribution and range between 50 and 230 mW/m^2 ($\mathcal{O} = 86 \text{ mW/m}^2$), which is in the range of previous estimates for the region^{3,7,15–17}. A band of high geothermal heat flow stretches from the south-western flank of the Byrd Subglacial Basin and Bentley Subglacial Trench, underlies most of the Thwaites and Pope glacier catchment and outflow areas and extends onto the inner and middle Amundsen Sea Embayment shelf. This high heat flow band is confined towards the eastern and western side by lower GHF values ranging from 50 to 80 mW/m^2 . We estimated the model uncertainties (Supplementary Fig. 4) based on the Curie depth standard deviation. By comparing this different GHF model outputs to the best-fit solution (Fig. 3a), the uncertainty distribution is predominantly 20 mW/m^2 or less and peaks up to 70 mW/m^2 south-east of Mount Takahe volcano. Further considerations are reported in Supplementary Discussion 2.2.

Geothermal heat flow data from continental rifts, such as the Baikal, Basin and Range, East African, Rhine and Rio Grande rifts, indicate that young rifts are characterized by high heat flow¹⁸. Mean values from the rift graben systems within rifts are typically in the range of $70\text{--}125 \text{ mW/m}^2$. In non-volcanic sections of the East African Rift System, heat flow is normal to low, but this system shows strong volcanic heat transport in its young rift grabens¹⁹.

The Amundsen Sea sector of the West Antarctic Rift System is characterized by recent or ongoing magmatic activity, which has been hypothesized for the Pine Island Glacier region²⁰ and the Executive Committee mountain range in Marie Byrd Land²¹. Further volcanic edifices are found to cluster in the southwestern flank of the BST, and beneath Thwaites glacier²². The absence of relevant seismicity²³ indicates that there is no active tectonism of the rift zone. Narrow regions of low seismic velocities in the upper mantle, for instance beneath the BST, may however infer a recent localized phase of extension²⁴.

High geothermal heat flow beneath Thwaites and Pope glaciers. Cumulative evidence, particularly the results from our study, points towards strongly elevated heat flow in the Amundsen Sea sector of the West Antarctic Rift System (Fig. 3a). The Moho is shallow with depths mostly between 17 and 32 km ^{25,26}, and its distribution correlates well with our Curie depth estimates. The thinned crust was attributed to Late Cretaceous/Early Cenozoic extensional phases²⁵, and is underlain by an upper mantle with presumably high temperatures in the depth range from 75 to 250 km ²⁷. The lithosphere is relatively thin ($<100 \text{ km}$), and density variations here predominantly stem from high upper mantle temperatures²⁸. Our shallow Curie depth estimates and inferred high heat flow correlate with areas of low lithospheric effective elastic thickness²⁹, T_e (Fig. 3b), indicative of a weak rifted lithosphere. The relatively high T_e estimates across the continental shelf are likely an effect of the up to 7 km thick sedimentary sequence of inferred early Cretaceous to Cenozoic age³⁰. The region of high T_e propagates east towards Thurston Island Block, which was part of a vast region along the formerly convergent paleo-Pacific margin stretching as a magmatic arc from the eastern Amundsen Sea sector to and along the western Antarctic Peninsula³¹. Regions of low T_e are prone to react more sensitively to changes in crustal loads. The observed glacial isostatic adjustment from ice mass loss in the Amundsen Sea sector exceed the uplift rates predicted from modeled glacial isostatic adjustment by more than 20 mm/year ³², suggesting a rapid upper mantle flow response. The highest measured uplift rates were found just west of Thwaites Glacier and near Pope Glacier in regions of low upper mantle viscosity³², which notably coincide with the region of our estimated high geothermal heat flow and low T_e (Fig. 3a, b).

Results of previous studies of Antarctic geothermal heat flow (Fig. 3c) vary strongly in their heat flow distribution and resolution for the Amundsen Sea sector. Heat flow based on continent-wide Curie depths³ was derived from the first edition of the Antarctic Digital Magnetic Anomaly Project (ADMAP)³³. The regional magnetic anomaly dataset presented in this study was not available for that compilation. Hence, their Curie depths for our study area

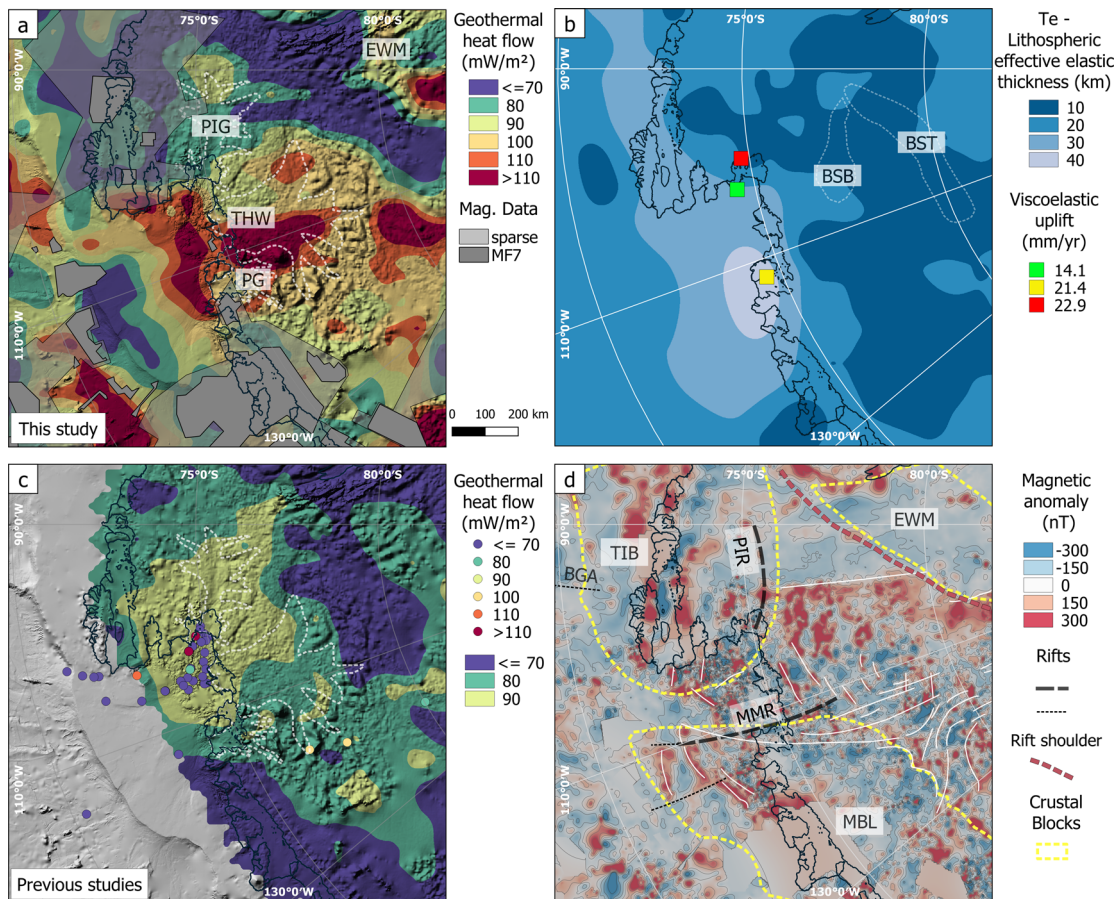


Fig. 3 Geothermal heat flow, lithospheric elastic thickness and magnetic anomaly distribution of the Amundsen Sea sector. **a** Geothermal heat flow distribution with areas of magnetic data gaps and those with MF7 magnetic data coverage (<https://www.geomag.us/models/MF7.html>) shown in gray. White dashed lines mark location of glaciers: PIG Pine Island glacier, THW Thwaites glacier, PG Pope glacier. **b** Lithospheric effective elastic thickness²⁹ and the visco-elastic response³². White dashed lines show area of Byrd subglacial basin (BSB) and Bentley subglacial trough (BST). **c** Compilation of continental-wide⁶ and local in-situ estimates of geothermal heat flow^{15,16,34,35}. **d** Tectonic features of the study region. The high geothermal heat flow region (A) is surrounded by the Thurston Island Block (TIB), Ellsworth-Whitmore Mountain (EWM) block and Marie Byrd Land (MBL). The Mount Murphy Rift (MMR)⁵⁴ correlates with a suite of NNE-SSW trending magnetic lineaments (marked with white lines). The Pine Island rift (PIR) is shown as part of the Thurston Island block.

mostly relied on satellite magnetic data that have lower spatial resolution, and therefore cannot resolve more local geothermal heat flow highs that we infer from aeromagnetic data in the Amundsen Sea sector. Other studies used radar echograms to interpret areas of basal melting for the estimation of geothermal heat flow in the Thwaites Glacier catchment⁷. Their GHF estimates are comparable to those of the continental scale models^{3,4}. GHF estimates from in-situ temperature gradient measurements lie within the lower end of that range^{15,16,34,35}. Our GHF results presented in this study yield a higher resolution estimate for this highly dynamic part of the West Antarctic Ice Sheet.

The elevated geothermal heat flow band (Fig. 3a) is interpreted as caused by an anomalously thin crust^{25,36}, underlain by a hot mantle^{26,27} and possible tectonic reactivation along older fault systems (e.g., Mount Murphy Rift). The magnetic anomaly grid reveals NNE-SSW trending lineaments located between the Thurston Island and Marie Byrd Land crustal blocks (Fig. 3d). These lineaments are regionally confined and attributed to the magnetic signature of Cenozoic rifting in the eastern branch of the West Antarctic Rift System. Crustal heterogeneity and magmatic intrusions are other likely contributors to the observed heat flow variability, for instance in the vicinity of Byrd Subglacial Basin. High seismic shear-wave velocities (>5 km/s) at 20 km depth may relate to lower crustal mafic intrusions³⁷ that likely

relate to subglacial volcanism²². Previous studies suggested that large, deep crustal plutons seated in extended continental crust may have formed rapidly but induced a prolonged perturbation of the deep-crustal geotherm³⁸.

The thermal anomalies, attributed to a thin and laterally heterogeneous rifted crust, magmatism and inferred fault reactivation, are likely to cause a heat-advection effect on the deep hydrological system and, therefore, exert a profound influence on the flow dynamics of the West Antarctic Ice Sheet in the Amundsen Sea sector. The direct transfer of heat can facilitate basal melting and control the ice rheology and basal sliding, and thus erosion³⁹. High geothermal heat flow beneath Thwaites and Pope glaciers could further contribute to rapid past and future changes in the glacier system. Our results in the Amundsen Sea region provide a new base for discussing the location and extent of crustal-scale thermal anomalies. This is a key finding to better characterize basal sliding properties and subglacial hydrology, as well as refine thermal boundary conditions for studies of ice sheet dynamics in the most rapidly changing sector of the West Antarctic Ice Sheet.

Methods

Magnetic anomaly dataset. The new magnetic anomaly grid for the Amundsen Sea sector of West Antarctica we compiled represents a further improvement with

respect to the latest generation of the publicly available ADMAP 2.0 Antarctic-wide magnetic anomaly grid⁴⁰. We integrated and processed existing offshore and onshore airborne magnetic anomaly data, unpublished onshore airborne data and data from new survey flights with detailed levelling to better constrain the lithospheric and crustal properties in the region. We expanded the AWI helicopter-magnetic anomaly grid⁴¹ with 14 flights (~2880 km total survey line length) on the continental shelf of the eastern Amundsen Sea Embayment during RV Polarstern expedition PS104⁴² (Supplementary Fig. 1). Furthermore, we added unpublished line data from the Pine Island Rift region and focused on cross-point calculations which exhibited a small offset (>50 nT). This step improved the data across the grounding lines of the Pine Island and Thwaites glaciers. Weather conditions did not allow for additional flights to link the onshore and offshore regions better. Additionally, a base station correction could not be applied to the helicopter-borne data offshore but was applied to all onshore data. Therefore, the data may still be affected by diurnal variations in the geomagnetic field. All magnetic data were DC shifted to the regional long-wavelength domain of the Magnetic Field Model MF7 (<https://www.geomag.us/models/MF7.html>) to help homogenize the long-wavelength magnetic field across different surveys⁴³. In areas, where no flight lines are available we also filled data gaps with the MF7 grid (Fig. 2a). A detailed description of the data and processing can be found in Supplementary Method 1.2.

Curie depth estimates. The depth-to-bottom of the magnetic source (Z_b) is in first approximation the Curie depth, which is considered as a proxy for geothermal heat flow, because of the temperature dependence of magnetization in crustal rocks. Regions found to have shallow Curie point depths are expected to have higher heat flow, and, therefore, higher average temperature gradients. Curie depth estimates mark transition zone, rather than an exact boundary, and assume a main magnetic source from magnetite with a Curie temperature of 550–580 °C^{44,45}. This assumption neglects the compositional variability in plutonic rocks that lead to Curie temperature ranges between 300 and 680 °C, and in cases of magnetic assemblages of Fe-Ni-Co-Cu metal alloys up to 620–1084 °C⁴⁶. Hence, we assume a temperature of 580 °C at the lowest magnetic boundary. We applied the centroid method after Tanaka et al.⁴⁷ to window sizes of 200 × 200 km and 300 × 300 km (Supplementary Figs. 2 and 3). The windows were extracted equidistantly from the newly compiled magnetic anomaly grid with a spacing of 50 km. We considered the fractal approach (power-law scaling) to calculate the Z_b as not applicable. High fractal scaling could underestimate Curie depths due to overcorrection⁴⁸ and has been discussed previously^{49,50}. From the slope of the power spectrum, the top boundary (Z_t) and the centroid of a magnetic layer (Z_0) composed of a horizontal (equivalent) layer are estimated (Supplementary Fig. 2). The basal depth of the magnetic source is $Z_b = 2Z_0 - Z_t$. The obtained bottom depth Z_b of the magnetic source is assumed to be the Curie point depth. The Curie depth error, which we calculated using the standard deviation from the spectral analysis, is less than ±2 km for most of the area (Supplementary Fig. 3).

Thermal modeling. A degree of uncertainty surrounds the mineralogical properties in the region. We therefore approximate the steady-state geothermal heat flow in a model of a homogenous material via

$$Q = -k \frac{\partial T}{\partial z}, \quad (1)$$

where Q is the heat flow at the bed surface (in mW/m²), T is the Curie temperature (580 °C), z the Curie depth (in km), and k the thermal conductivity of the lithosphere (in W/mK). The resulting geothermal heat flow thus represents a linear transformation of the Curie depth map.

Data availability

The datasets collected for and generated in this study are available from PANGAEA Data Publisher (www.pangaea.de). The link is <https://doi.org/10.1594/PANGAEA.932452>.

Received: 22 February 2021; Accepted: 22 July 2021;

Published online: 18 August 2021

References

- Fisher, A. T. et al. High geothermal heat flux measured below the West Antarctic Ice Sheet. *Sci. Adv.* **1**, e1500093 (2015).
- Fox Maule, C., Purucker, M. E., Olsen, N. & Mosegaard, K. Heat flux anomalies in Antarctica revealed by satellite magnetic data. *Science* **309**, 464–467 (2005).
- Martos, Y. M. et al. Heat flux distribution of Antarctica unveiled. *Geophys. Res. Lett.* **44**, 11417–11426 (2017).
- Shapiro, N. & Ritzwoller, M. H. Inferring surface heat flux distributions guided by a global seismic model: particular application to Antarctica. *Earth Planet. Sci. Lett.* **223**, 213–224 (2004).
- An, M. et al. Temperature, lithosphere-asthenosphere boundary, and heat flux beneath the Antarctic Plate inferred from seismic velocities. *J. Geophys. Res. Solid Earth* **120**, 8720–8742 (2015).
- Shen, W., Wiens, D. A., Lloyd, A. J. & Nyblade, A. A. A geothermal heat flux map of Antarctica empirically constrained by seismic structure. *Geophys. Res. Lett.* **47**, 1–8 (2020).
- Schroeder, D. M., Blankenship, D. D., Young, D. A. & Quartini, E. Evidence for elevated and spatially variable geothermal flux beneath the West Antarctic Ice Sheet. *Proc. Natl. Acad. Sci.* **111**, 9070–9072 (2014).
- Burton-Johnson, A., Halpin, J. A., Whittaker, J. M., Graham, F. S. & Watson, S. J. A new heat flux model for the Antarctic Peninsula incorporating spatially variable upper crustal radiogenic heat production. *Geophys. Res. Lett.* **44**, 5436–5446 (2017).
- Dalziel, I. W. D. On the extent of the active West Antarctic rift system. *Terra Antartica Rep.* **12**, 193–202 (2006).
- Müller, R. D., Gohl, K., Cande, S. C., Goncharov, A. & Golynsky, A. V. Eocene to Miocene geometry of the West Antarctic Rift System. *Aust. J. Earth Sci.* **54**, 1033–1045 (2007).
- Granot, R., Cande, S. C., Stock, J. M. & Damaske, D. Revised Eocene-Oligocene kinematics for the West Antarctic rift system. *Geophys. Res. Lett.* **40**, 279–284 (2013).
- Joughin, I., Smith, B. E. & Medley, B. Marine ice sheet collapse potentially underway for the Thwaites Glacier Basin, West Antarctica. *Science* **344**, 735–738 (2014).
- Rignot, E., Mouginot, J., Morlighem, M., Seroussi, H. & Scheuchl, B. Widespread, rapid grounding line retreat of Pine Island, Thwaites, Smith, and Kohler glaciers, West Antarctica, from 1992 to 2011. *Geophys. Res. Lett.* **41**, 3502–3509 (2014).
- Rignot, E. et al. Four decades of Antarctic Ice Sheet mass balance from 1979–2017. *Proc. Natl. Acad. Sci.* **116**, 1095–1103 (2019).
- Dziadek, R., Gohl, K. & Kaul, N. Elevated geothermal surface heat flow in the Amundsen Sea Embayment, West Antarctica. *Earth Planet. Sci. Lett.* **506**, 530–539 (2019).
- Dziadek, R., Gohl, K., Diehl, A. & Kaul, N. Geothermal heat flux in the Amundsen Sea sector of West Antarctica: New insights from temperature measurements, depth to the bottom of the magnetic source estimation, and thermal modeling. *Geochem. Geophys. Geosyst.* **18**, 2657–2672 (2017).
- Damiani, T. M., Jordan, T. A., Ferraccioli, F., Young, D. A. & Blankenship, D. D. Variable crustal thickness beneath Thwaites Glacier revealed from airborne gravimetry, possible implications for geothermal heat flux in West Antarctica. *Earth Planet. Sci. Lett.* **407**, 109–122 (2014).
- Morgan, P. Constraints on rift thermal processes from heat flow and uplift. *Dev. Geotecton.* **19**, 277–298 (1983).
- Lucazeau, F. Analysis and mapping of an updated terrestrial heat flow dataset. *Geochem. Geophys. Geosyst.* **20**, 4001–4024 (2019).
- Loose, B. et al. Evidence of an active volcanic heat source beneath the Pine Island Glacier. *Nat. Commun.* **9**, 1–9 (2018).
- Lough, A. et al. Seismic detection of an active subglacial magmatic complex in Marie Byrd Land, Antarctica. *Nat. Geosci.* **6**, 1031–1035 (2013).
- van Wyk de Vries, M., Bingham, R. G. & Hein, A. S. A new volcanic province: an inventory of subglacial volcanoes in West Antarctica. *Geol. Soc. London, Spec. Publ.* **461**, <https://doi.org/10.1144/SP461.7> (2018).
- Winberry, J. P. & Anandakrishnan, S. Seismicity and neotectonics of West Antarctica. *Geophys. Res. Lett.* **30**, 1931 (2003).
- Lloyd, A. J. et al. A seismic transect across West Antarctica: evidence for mantle thermal anomalies beneath the Bentley Subglacial Trench and the Marie Byrd Land Dome. *J. Geophys. Res. Solid Earth* **120**, 8439–8460 (2015).
- Jordan, T. A. et al. Aerogravity evidence for major crustal thinning under the Pine Island Glacier region (West Antarctica). *Geol. Soc. Am. Bull.* **122**, 714–726 (2010).
- Shen, W. et al. The crust and upper mantle structure of Central and West Antarctica from Bayesian inversion of Rayleigh wave and receiver functions. *J. Geophys. Res. Solid Earth* **123**, 7824–7849 (2018).
- Lloyd, A. J. et al. Seismic structure of the Antarctic upper mantle based on adjoint tomography. *J. Geophys. Res. Solid Earth* **120**, 8439–8460 <https://doi.org/10.1029/2019JB017823> (2019).
- Haeger, C., Kaban, M. K., Tesauro, M., Petrunin, A. G. & Mooney, W. D. 3-D density, thermal, and compositional model of the Antarctic lithosphere and implications for its evolution. *Geochem. Geophys. Geosyst.* **20**, 688–707 (2019).
- Chen, B., Haeger, C., Kaban, M. K. & Petrunin, A. G. Variations of the effective elastic thickness reveal tectonic fragmentation of the Antarctic lithosphere. *Tectonophysics* **746**, 412–424 (2018).
- Gohl, K. et al. Seismic stratigraphic record of the Amundsen Sea Embayment shelf from pre-glacial to recent times: evidence for a dynamic West Antarctic ice sheet. *Mar. Geol.* **344**, 115–131 (2013).
- Zundel, M., Spiegel, C., Lisker, F. & Monien, P. Post-mid-Cretaceous tectonic and topographic evolution of western Marie Byrd Land, West Antarctica:

- insights from apatite fission track and (U-Th-Sm)/He data. *Geochim. Geophys. Geosyst.* **20**, 5831–5848 (2019).
32. Groh, A. et al. An investigation of glacial isostatic adjustment over the Amundsen Sea sector, West Antarctica. *Glob. Planet. Change* **98–99**, 45–53 (2012).
 33. Golynsky, A. et al. ADMAP - A Digital Magnetic Anomaly Map of the Antarctic, in *Antarctica* (eds. Fütterer, D. K. et al.) 109–116 (Springer, 2006).
 34. Clow, G. D., Cuffey, K. M. & Waddington, E. D. High heat-flow beneath the central portion of the West Antarctic Ice Sheet. In: *Proceedings of the American Geophysical Union*, abstract C31A-0577 (AGU Fall Meeting, 2012).
 35. Gow, A. J., Ueda, H. & Garfield, D. Antarctic ice sheet: preliminary results of the first core to bedrock. *Science* **161**, 1013–1101 (1968).
 36. Pappa, F., Ebbing, J. & Ferraccioli, F. Moho depths of Antarctica: comparison of seismic, gravity, and isostatic results. *Geochim. Geophys. Geosyst.* **20**, 1629–1645 (2019).
 37. O'Donnell, J. P. et al. Mapping crustal shear wave velocity structure and radial anisotropy beneath West Antarctica using seismic ambient noise. *Geochim. Geophys. Geosyst.* **20**, 5014–5037 (2019).
 38. Peressini, G., Quick, J. E., Sinigoi, S., Hofmann, A. W. & Fanning, M. Duration of a large mafic intrusion and heat transfer in the lower crust: a SHRIMP U-Pb zircon study in the Ivrea-Verbano Zone (Western Alps, Italy). *J. Petrol.* **48**, 1185–1218 (2007).
 39. Fahnestock, M., Abdalati, W., Joughin, I., Brozena, J. & Gogineni, P. High geothermal heat flow, basal melt, and the origin of rapid ice flow in central Greenland. *Science* **294**, 2338–2342 (2001).
 40. Golynsky, A. V. et al. New magnetic anomaly map of the Antarctic. *Geophys. Res. Lett.* **45**, 6437–6449 (2018).
 41. Gohl, K., Denk, A., Eagles, G. & Wobbe, F. Deciphering tectonic phases of the Amundsen Sea Embayment shelf, West Antarctica, from a magnetic anomaly grid. *Tectonophysics* **585**, 113–123 (2013).
 42. Gohl, K. The Expedition PS104 of the Research Vessel POLARSTERN to the Amundsen Sea in 2017. *Reports on Polar and Marine Research* **712** (Alfred Wegener Institute, 2017).
 43. Ebbing, J., Yixiati, D., Haas, P., Ferraccioli, F. & Scheiber-Enslin, S. East Antarctica magnetically linked to its ancient neighbours in Gondwana. *Sci. Rep.* **11**, <https://doi.org/10.1038/s41598-021-84834-1> (2021).
 44. Bansal, A. R., Gabriel, G., Dimri, V. P. & Krawczyk, C. M. Estimation of depth to the bottom of magnetic sources by a modified centroid method for fractal distribution of sources: an application to aeromagnetic data in Germany. *Geophysics* **76**, L11–L22 (2011).
 45. Li, C. F., Lu, Y. & Wang, J. A global reference model of Curie-point depths based on EMAG2. *Sci. Rep.* **7**, <https://doi.org/10.1038/srep45129> (2017).
 46. Haggerty, S. E. Mineralogical constraints on curie isotherms in deep crustal magnetic anomalies. *Geophys. Res. Lett.* **5**, 105–108 (1978).
 47. Tanaka, A., Okubo, Y. & Matsubayashi, O. Curie point depth based on spectrum analysis of the magnetic anomaly data in East and Southeast Asia. *Tectonophysics* **306**, 461–470 (1999).
 48. Li, C. F., Zhou, D. & Wang, J. On application of fractal magnetization in Curie depth estimation from magnetic anomalies. *Acta Geophys.* **67**, 1319–1327 (2019).
 49. Bansal, A. R., Anand, S. P., Rajaram, M., Rao, V. K. & Dimri, V. P. Depth to the bottom of magnetic sources (DBMS) from aeromagnetic data of Central India using modified centroid method for fractal distribution of sources. *Tectonophysics* **603**, 155–161 (2013).
 50. Chen, G., Cheng, Q. & Zhang, H. Matched filtering method for separating magnetic anomaly using fractal model. *Comput. Geosci.* **90**, 179–188 (2016).
 51. Morlighem, M. et al. Deep glacial troughs and stabilizing ridges unveiled beneath the margins of the Antarctic ice sheet. *Nat. Geosci.* **13**, 132–137 (2020).
 52. Mouginot, J., Scheuch, B. & Rignot, E. Mapping of ice motion in Antarctica using synthetic-aperture radar data. *Remote Sens.* **4**, 2753–2767 (2012).
 53. Rignot, E., Mouginot, J. & Scheuchel, B. Ice flow of the Antarctic Ice Sheet. *Science* **333**, 1427–1430 (2011).
 54. Spiegel, C. et al. Tectonomorphic evolution of Marie Byrd Land—implications for Cenozoic rifting activity and onset of West Antarctic glaciation. *Glob. Planet. Change* **145**, 98–115 (2016).

Acknowledgements

We are grateful to Don Blankenship, Duncan Young, and John Holt of University of Texas—Austin for providing airborne magnetic data they collected as part of the AGASEA project in 2006. The magnetic field model MF7 was obtained from the project webpage (www.geomag.us/models/MF7.html). Many thanks to the master and crew of RV Polarstern Expedition PS104 (2017) for their support. This study was supported by the Deutsche Forschungsgemeinschaft (DFG) in the framework of the Priority Program 1158 “Antarctic research with comparative investigations in Arctic ice areas” by grant GO 724/14-1 to K.G. Additional funds were contributed by the AWI through its research programs PACES-II Workpackage 3.2 and Changing Earth—Sustaining our Future, Subtopic 2.3. The work of F.F. for this paper is a contribution to the 3D Earth (ADMAP 2.0+ CCN) and 4D Antarctica projects of ESA on the Antarctic lithosphere and its influence on subglacial geothermal heat flow, respectively. F.F. acknowledges in particular ESA financial support for several visits to AWI, where joint aeromagnetic anomaly data processing and interpretation was performed. Our study contributes to the Scientific Research Program “Instabilities & Thresholds in Antarctica” (INSTANT) of the Scientific Committee for Antarctic Research (SCAR). We would like to thank two anonymous reviewers for their very constructive and helpful comments, which benefited the manuscript considerably.

Author contributions

R.D. contributed with conceptualization, writing, original draft preparation, visualization. All authors conducted the data acquisition and analysis. F.F. contributed with the joint aeromagnetic anomaly data processing and interpretation. K.G. was responsible for supervision, project administration, and funding acquisition. All authors have read and agreed to the published version of the manuscript.

Funding

Open Access funding enabled and organized by Projekt DEAL.

Competing interests

The authors declare no competing interests.

Additional information

Supplementary information The online version contains supplementary material available at <https://doi.org/10.1038/s43247-021-00242-3>.

Correspondence and requests for materials should be addressed to K.G.

Peer review information *Communications Earth & Environment* thanks the anonymous reviewers for their contribution to the peer review of this work. Primary Handling Editors: Joe Aslin, Heike Langenberg.

Reprints and permission information is available at <http://www.nature.com/reprints>

Publisher's note Springer Nature remains neutral with regard to jurisdictional claims in published maps and institutional affiliations.



Open Access This article is licensed under a Creative Commons Attribution 4.0 International License, which permits use, sharing, adaptation, distribution and reproduction in any medium or format, as long as you give appropriate credit to the original author(s) and the source, provide a link to the Creative Commons license, and indicate if changes were made. The images or other third party material in this article are included in the article's Creative Commons license, unless indicated otherwise in a credit line to the material. If material is not included in the article's Creative Commons license and your intended use is not permitted by statutory regulation or exceeds the permitted use, you will need to obtain permission directly from the copyright holder. To view a copy of this license, visit <http://creativecommons.org/licenses/by/4.0/>.

© The Author(s) 2021